

Aeolian erosion in protoplanetary discs: How impactful it is on dust evolution?

Stéphane Michoulier¹, Jean-François Gonzalez¹, Evgeni Grishin², and Clément Petetin¹

¹ Université Claude Bernard Lyon 1, CRAL UMR5574, ENS de Lyon, CNRS, Villeurbanne, F-69622, France
e-mail: jean-francois.gonzalez@ens-lyon.fr

² Monash Centre for Astrophysics (MoCA) and School of Physics and Astronomy, Monash University, Vic. 3800, Australia

Received 13 November 2023; accepted 26 February 2024

ABSTRACT

Context. Many barriers prevent dust to form planetesimals via coagulation in protoplanetary discs, such as bouncing, collisional fragmentation or aeolian erosion. Modelling dust and the different phenomena that can alter its evolution is therefore needed. Multiple solutions have been proposed, but still need to be confirmed.

Aims. In this paper, we explore the role aeolian erosion plays in the evolution of dust.

Methods. We use a monodisperse model to account for dust growth and fragmentation, implemented in a 1D model to compute the evolution of single grains and a 3D SPH code to compute the global evolution of dust and gas. We test the erosion model in our code and ensured it matches previous results.

Results. With a model of disc reproducing observations, we show with both 1D and 3D studies that erosion is not significant during the evolution of dust when we take fragmentation into consideration. With a low-viscosity disc, fragmentation is less of a problem, but grain growth is also less important, preventing the formation of large objects anyway. In dust traps, close to the star, erosion is also not impactful, even when fragmentation is turned off.

Conclusions. We show in this paper that aeolian erosion is negligible when radial drift, fragmentation and dust traps are taken into account and does not alter the dust evolution in the disc. However, it can have an impact on later stages, i.e. when the streaming instability forms large clumps close to the star, or when planetesimals are captured.

Key words. methods: numerical – planets and satellites: formation – protoplanetary discs

1. Introduction

Protoplanetary discs consist of gas and dust that orbit young stars and provide the necessary material for the agglomeration and growth of planetesimals, the building blocks of planets. The dynamical and physical processes occurring within these discs play a crucial role in shaping the characteristics and composition of planetary systems. Among these processes, aeolian erosion of large dust particles might influence the dynamics and evolution of the dust in the inner regions of protoplanetary discs (Blum & Wurm 2000; Wurm et al. 2001).

Aeolian erosion is a process where dust particles are ejected from a larger object due to the combined action of gas drag and turbulent motions within the disc. It has been studied by Blum & Wurm (2000); Wurm et al. (2001); Paraskov et al. (2006), and more recently by Rozner et al. (2020) and Grishin et al. (2020) (hereafter R20 and G20). They showed that large aggregates can be eroded in a short time, typically ranging from a few years to a few thousand years, with sizes going from several hundred metres down to a couple of centimetres (R20; G20). This process is therefore believed to destroy large boulders very efficiently and impact the evolution of grains in the inner region of the disc. Hence, erosion is another barrier to dust growth from small sizes to kilometeric objects.

In addition to aeolian erosion, fragmentation of dust particles is a process that can destroy grains in the inner regions of protoplanetary discs. When dust particles collide at high velocities, they may experience catastrophic disruptions, leading to the

so-called fragmentation barrier (Weidenschilling & Cuzzi 1993; Dominik & Tielens 1997; Blum & Wurm 2008). Fragmentation thresholds or material properties to model collisions are still not fully understood, with many uncertainties remaining. Moreover, dust experiences radial drift during its growth in the disc due to gas drag. Grains of a few centimetres to metres drift very efficiently, due to marginal coupling to the gas, and are accreted onto the star (Whipple 1972), which defines the radial drift barrier (Weidenschilling 1977). In order to prevent radial drift and the loss of material onto the star, several solutions have been proposed in order to help the formation of planetesimals. Some rely on the capture of dust in pressure maxima, others bypass the barriers to dust growth. For instance, vortices have been explored (Barge & Sommeria 1995; Meheut et al. 2012; Loren-Aguilar & Bate 2015) to trap dust and form clumps directly from gravitational collapse. Snow lines (Kretke & Lin 2007; Brauer et al. 2008; Drażkowska et al. 2014; Vericel & Gonzalez 2020) and self-induced dust traps (Gonzalez et al. 2017; Vericel & Gonzalez 2020; Vericel et al. 2021) form local pressure maxima, stopping the radial drift and helping grain growth by the increase of the local dust density. Other properties of dust have also been investigated like grain porosity (Ormel et al. 2007; Suyama et al. 2008; Okuzumi et al. 2009, 2012; Kataoka et al. 2013; Garcia & Gonzalez 2020), allowing grains to grow faster and to larger sizes, while being less sensitive to fragmentation. Additionally, other processes related to instabilities have been under investigation these recent years, mostly with the streaming instability (Youdin & Goodman 2005; Youdin & Johansen 2007;

Yang et al. 2017; Schäfer et al. 2017; Auffinger & Laibe 2018; Li et al. 2019) which allows dust to directly form boulders from pebbles, bypassing the different barriers grains might undergo during their evolution. Grishin et al. (2019) looked at a different solution where planetesimals can be captured in protoplanetary discs early. This had also been shown to occur in earlier stages, such as molecular clouds (Pfalzner & Bannister 2019; Pfalzner et al. 2021).

In this paper, we study the importance of aeolian erosion in relation to fragmentation and its importance in disc inner regions. In a previous paper, we compared the importance of fragmentation and rotational disruption of porous grains (Michoulier & Gonzalez 2022), a new barrier introduced by Tatsuuma & Kataoka (2021). In this paper, however, we will not take into account porosity as the current model for aeolian erosion of R20 and G20 does not take into account the evolution of density. We will therefore limit ourselves to the simpler compact grains formalism.

The paper is built as follows: we first describe our dust growth and fragmentation model and introduce the model to take aeolian erosion into account in Sect. 2. We then show the tests performed to make sure the implementation of the erosion module is correctly done in Sect. 3. Then, we discuss the results in Sect. 4 using the 1D code PAMDEAS¹ (Michoulier & Gonzalez 2022) and the 3D code PHANTOM by Price et al. (2018) to show the unimportance of aeolian erosion with respect to fragmentation. Finally, we discuss our results about erosion and the limitations of the codes in Sect. 5, and end with a conclusion in Sect. 6.

2. Methods

To determine the importance of different barriers, we describe in the following how growth, fragmentation and erosion are taken into account in PAMDEAS. When using PHANTOM (Price et al. 2018), all the details about the implementation of growth and fragmentation are presented in Vericel et al. (2021). The erosion model implemented in PAMDEAS and PHANTOM is the same, and the growth and fragmentation models are identical, but the implementation differs slightly and are code-related.

2.1. Dust grain growth model

In order to model dust growth, we consider a locally uniform mass distribution of grains where collisions occur exclusively between grains of identical mass. The equation describing the size variation is given by Stepinski & Valageas (1997):

$$\left(\frac{ds}{dt}\right)_{\text{grow}} = \frac{\rho_d}{\rho_s} v_{\text{rel}}. \quad (1)$$

where ρ_d is the dust local density, ρ_s the grain intrinsic density and v_{rel} , relative velocity during collision, is:

$$v_{\text{rel}} = \sqrt{2^{3/2} \text{Ro}} \alpha c_g \frac{\sqrt{\text{St}}}{1 + \text{St}}. \quad (2)$$

α is the turbulent viscosity parameter (Shakura & Sunyaev 1973) and c_g is the gas sound speed. St is the Stokes number usually defined as the dimensionless stopping time, $\Omega_K t_s$, where Ω_K is the Keplerian frequency and t_s the drag stopping time. St quantifies the coupling between gas and dust, which depends on the drag

regimes and the grain size ($\text{St} \propto s$ in the Epstein regime). Ro, the Rossby number, is considered to be a constant equal to 3 (Stepinski & Valageas 1997). Full details of the model and its derivation are presented in Laibe et al. (2008); Gonzalez et al. (2015, 2017) or Vericel et al. (2021). Naturally, the growth rate increases as the relative velocity increases, as this enhances the probability of collision occurrence. Moreover, the growth rate exhibits a linear dependence on ρ_d , indicating that the settling of dust grains or their accumulation in dust traps favour dust growth.

2.2. Fragmentation

When the relative velocity between grains exceeds a critical threshold known as v_{frag} , instead of growing, the grains undergo fragmentation, as observed by Tanaka et al. (1996). The impact's kinetic energy becomes too high for the grain's structure to absorb, causing the bonds between the constituent monomers of the aggregate to break apart. To quantify the mass variation during fragmentation, we can adopt a formulation similar to that proposed by Stepinski & Valageas (1997) for growth. Using a realistic approach developed by Kobayashi & Tanaka (2010) and Garcia (2018) and further used by Vericel et al. (2021), the model introduces a concept of progressive or ‘‘soft’’ fragmentation, taking into account the relative velocity (v_{rel}) compared to v_{frag} :

$$\left(\frac{ds}{dt}\right)_{\text{frag}} = -\frac{v_{\text{rel}}^2}{v_{\text{rel}}^2 + v_{\text{frag}}^2} \frac{\rho_d}{\rho_s} v_{\text{rel}}. \quad (3)$$

When the relative velocity is near the fragmentation threshold, the mass loss becomes less pronounced. Therefore, a fragmenting grain loses approximately half of its initial mass after a collision time² when $v_{\text{rel}} = v_{\text{frag}}$ or more when $v_{\text{rel}} > v_{\text{frag}}$. When $v_{\text{rel}} \gg v_{\text{frag}}$, the situation described by Gonzalez et al. (2015) is recovered, where the entire grain fragments, losing most of its mass within a collision time.

2.3. Aeolian erosion

R20 and G20 considered aeolian erosion by gas as a mechanism to reduce the size of large aggregates when they are decoupled from the gas. The following section is inspired by those works. During erosion, grains of size s_{ej} are ejected from the original aggregate of size s ranging from one metre to one kilometre. If we consider a surrounding gas density ρ_g and a velocity difference between dust and gas Δv , the characteristic time for a grain to be ejected is given by:

$$t_{\text{ej}} = \frac{\Delta v}{a_{\text{coh}}}, \quad (4)$$

where a_{coh} is the cohesive acceleration required for the grain to remain attached. The work exerted by the gas on the aggregate and the energy loss due to erosion are given by R20:

$$W = p \Delta v A t_{\text{ej}}, \quad (5)$$

$$\Delta E = -\Delta m \frac{\Delta v^2}{2}, \quad (6)$$

² It is worth noting that our definition of fragmentation aligns with the point at which half of the mass is lost. However, it's important to acknowledge that other definitions exist. For example, Ringl et al. (2012); Gunkelmann et al. (2016) define fragmentation as the moment when at least one monomer is ejected from the main aggregate. We refer to the loss of grain mass when it's less than half of the initial mass as erosion.

¹ <https://github.com/StephaneMichoulier/Pamdeas.git>

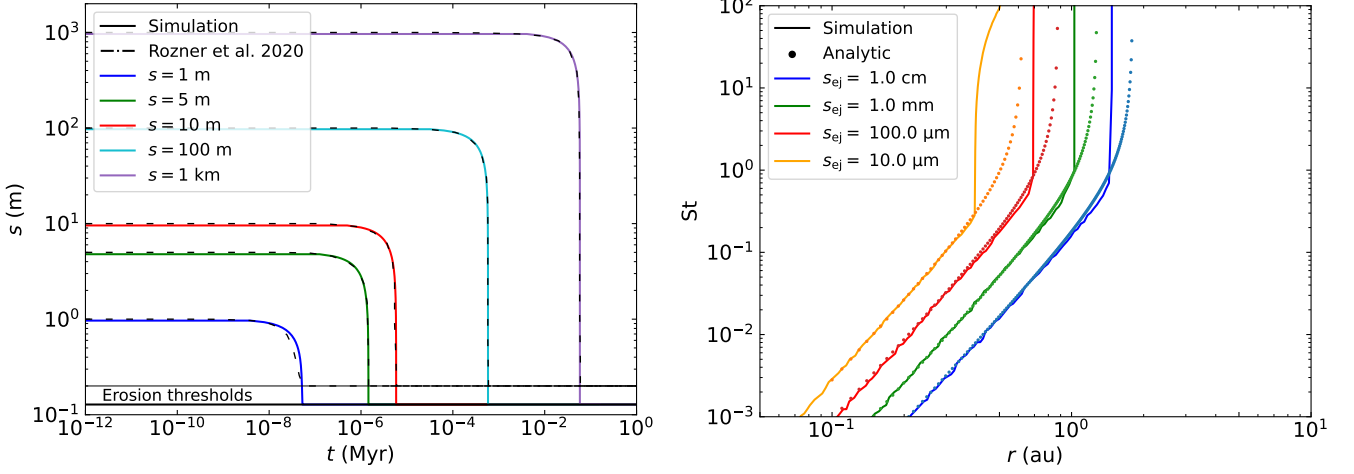


Fig. 1. **Left:** Time evolution of the size s of different aggregates as they are eroded. The vertical turnover in the profile gives the characteristic erosion time. The aggregates are kept at a fixed distance of 1 au from the star, and the ejected dust has a size of $100 \mu\text{m}$. Dashed lines represent data from R20, which are in excellent agreement with our results. **Right:** Stokes number at the erosion threshold for aggregates drifting towards the star and four different sizes of ejected grains. Dotted lines represent the analytical solution presented in G20.

where $p = \frac{1}{2}\rho_g\Delta v^2$ is the dynamic pressure and A is the effective shear surface. Since work and energy loss are equal, the mass loss is then:

$$\Delta m = -A\rho_g \frac{\Delta v^2}{a_{\text{coh}}}. \quad (7)$$

In the case of an infinitesimal time interval $dt < t_{ej}$, $A \approx s\Delta v dt$, the mass loss becomes

$$\left(\frac{dm}{dt}\right)_{\text{eros}} = -\rho_g \frac{\Delta v^3}{a_{\text{coh}}} s. \quad (8)$$

Currently, a_{coh} is an unknown but Shao & Lu (2000) showed that the cohesive force could be related to a_{coh} .

$$F_{\text{coh}} = m_{ej}a_{\text{coh}} = \beta_{\text{eros}}s_{ej}, \quad (9)$$

where m_{ej} is the mass of an ejected grain and β_{eros} is a parameter to define. The experimental measurements of β_{eros} by Heim et al. (1999) and Paraskov et al. (2006) show a strong cohesive force, resulting in a value of $\beta_{\text{eros}} = 0.1 \text{ kg}\cdot\text{s}^{-2}$. With this relation between a_{coh} and β_{eros} , we can finally rewrite Eq. (8) in terms of size loss as:

$$\left(\frac{ds}{dt}\right)_{\text{eros}} = \frac{-\rho_g s_{ej}^2 \Delta v^3}{3 s \beta_{\text{eros}}}. \quad (10)$$

This equation will be used in the simulations to determine the importance of erosion. However, for erosion to occur, the erosion threshold must first be reached. This threshold was determined by Shao & Lu (2000) and is expressed as:

$$\Delta v_{\text{eros}} = \sqrt{A_N \frac{\gamma_s}{\rho_g s_{ej}}}, \quad (11)$$

where $A_N = 0.0123$ is a numerical constant and $\gamma_s = 1.65 \times 10^{-4} \text{ J m}^{-2}$, the surface energy, is the same as in R20. Δv_{eros} thus depends essentially on s_{ej} .

In this work, $\Delta v = v_d - v_g$, the velocity difference between dust and gas is given by:

$$\Delta v_r = \frac{(1 + \varepsilon)St}{(1 + \varepsilon)^2 + St^2} v_{\text{drift}} - \frac{St^2}{(1 + \varepsilon)^2 + St^2} v_{\text{visc}}, \quad (12)$$

$$\Delta v_\theta = -\frac{St^2}{(1 + \varepsilon)^2 + St^2} \frac{v_{\text{drift}}}{2} - \frac{(1 + \varepsilon)St}{(1 + \varepsilon)^2 + St^2} \frac{v_{\text{visc}}}{2}, \quad (13)$$

where ε is the dust-to-gas ratio, v_{drift} is the radial drift velocity associated to the gas pressure gradient, and v_{visc} is the one due to gas motion caused by viscosity (full details on the derivation can be found in Michoulier & Gonzalez 2022). Δv is hence given by $\Delta v = \sqrt{\Delta v_r^2 + \Delta v_\theta^2}$, and is compared to the erosion threshold Δv_{eros} .

3. Tests

To ensure that our implementation of the equations describing erosion works as intended, we conduct tests to compare our results with those of R20 and G20, as shown in Fig. 1. To conduct these tests, we use the same disc parameters, which correspond to a Minimum Mass Solar Nebula model (Perets & Murray-Clay 2011; Grishin & Perets 2015). The surface density is $\Sigma_g = 2 \times 10^4 (r/r_0)^{-1.5} \text{ kg m}^{-2}$, and the temperature $T_g = 120 (r/r_0)^{-3/7} \text{ K}$, with $r_0 = 1 \text{ au}$. This gives an aspect ratio $H/r = 0.022 (r/r_0)^{2/7}$ and a gas density $\rho_g \approx 3 \times 10^{-6} (r/r_0)^{-16/7} \text{ kg m}^{-3}$. The dust-to-gas ratio is small and does not play a role here. Figure 1 on the left demonstrates that our simulations using PAMDEAS perfectly reproduce the data from Figure 4 of R20. The characteristic erosion timescale for each aggregate size is accurately reproduced. When $\Delta v_{\text{eros}} = \Delta v$, as the distance is kept fixed, the erosion threshold corresponds to only one value of St and hence one size. It should be noted that the size at which the erosion threshold is reached is slightly different (127 cm instead of 200 cm in R20). This difference likely arises from the way Δv is computed, which differs between this work and R20 and G20. Although the physical size is different, what determines the relative velocity is the Stokes number, which is the same, as shown in the right panel.

On the right, Fig. 1 shows the critical Stokes number (St) at the erosion threshold. In this case, the grains to be eroded have an initial size of 10 metres, and are initially placed in the outer disc. Grains then drift toward the star until they cross the erosion threshold. The data are compared with the analytical solution that give the erosion threshold in terms of critical Stokes number, a polynomial of degree 5, which takes into account both laminar and turbulent gas flow (see Eq. (8) in G20) around the aggregate. To achieve this, one writes the sum of Δv for laminar

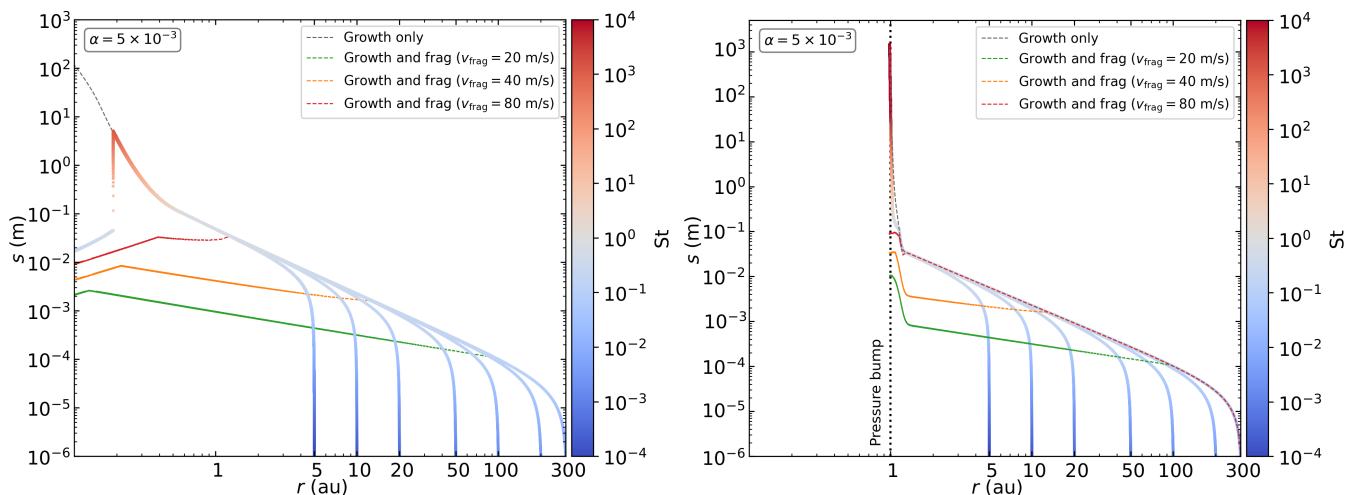


Fig. 2. **Left:** Evolution of the size s of grains experiencing growth and erosion only, as they grow and drift inwards from different initial distances r from the star. The colour represents the Stokes number. The gray dashed line represents the evolution without erosion, and the green, orange and red lines represent the evolution with growth and fragmentation using a fragmentation threshold of 20, 40 and 80 m s^{-1} . The size of the ejected grains is $s_{\text{ej}} = 1 \text{ mm}$, a typical value used by R20 and G20. **Right:** Same as the left panel, but with a pressure maximum that traps dust at 1 au.

and turbulent gas flow as a function of St , which equals Δv_{eros} at the erosion threshold, and then numerically solves for St . As the size of the ejected grains increase, erosion becomes easier as erosion starts at larger distances r compared to smaller s_{ej} . The simulations also show excellent agreement with the analytical solution. The difference occurs at large St and is due to the fact that a grain evolving in PAMDEAS takes a non-zero time to be eroded and reach the equilibrium.

4. Results

4.1. Setup

To be closer to reality than the Minimum Mass Solar Nebula (MMSN) model, we use a disc model that reproduces observations, presented in Williams & Best (2014). For PAMDEAS, the masses of the star and of the disc are set to $M_* = 1 M_{\odot}$ and $M_{\text{disc}} = 0.01 M_{\odot}$. The inner and outer radii are $R_{\text{in}} = 0.1 \text{ au}$ and $R_{\text{out}} = 300 \text{ au}$, while the disc aspect ratio is $H/R_0 = 0.0895$ with a reference radius $R_0 = 100 \text{ au}$. The density and temperature profiles exponents are $p = 1$ and $q = 0.5$. The turbulent viscosity parameter (Shakura & Sunyaev 1973) is set to $\alpha = 5 \times 10^{-3} - 5 \times 10^{-4}$. A typical dust-to-gas ratio of 1% is used. We use silicates with $\rho_s = 2.7 \text{ kg m}^{-3}$ and initial size $s_0 = 1 \mu\text{m}$, with different fragmentation thresholds $v_{\text{frag}} = 20-40-80 \text{ m s}^{-1}$. For erosion, we use $\beta_{\text{eros}} = 0.1 \text{ kg.s}^{-2}$, and the ejected grain size $s_{\text{ej}} = 1 \text{ mm}$, the largest physical value to maximise the effect of erosion (R20; G20), as smaller s_{ej} would reduce $\left(\frac{ds}{dt}\right)_{\text{eros}} \propto s_{\text{ej}}^2$. In addition, one of the assumptions in the erosion model is that the cohesive force F_{coh} is proportional to the grain size, which, according to G20 is valid up to 1 mm. Hence, we will only use this value in this paper. To model a pressure bump centred at 1 au, we simply add to the initial profile a Gaussian with a width of 0.1 au and a height of 20 times the initial surface at 1 au. The local dust-to-gas ratio in the pressure bump is set to 1, a typical value expected in dust traps where dust is settled and concentrated. As 3D simulations are more expensive, we only model the inner disc with PHANTOM, keeping M_* and R_{in} the same but taking $R_{\text{out}} = 5 \text{ au}$ and $R_0 = 1 \text{ au}$, which gives $M_{\text{disc}} = 1.64 \times 10^{-4} M_{\odot}$ in order to have the same surface density, with $\alpha = 5 \times 10^{-3}$. We use for all 3D simulations 10^6 particles. Simulations start with

gas only, in order to prevent artefacts due to gas relaxation. After 10 orbits at 5 au ($\sim 120 \text{ yr}$), the disc is relaxed, and dust is added with a uniform dust-to-gas ratio of 1%, and the grain size is initialized at $s = 100 \mu\text{m}$, with $v_{\text{frag}} = 80 \text{ m s}^{-1}$. The other parameters remain the same.

4.2. 1D study

In R20 and G20, erosion near the star is presented for certain aggregate sizes. Aggregates on the order of metres can be easily eroded into centimetre sized aggregates, particularly with large ejected grains. With $\alpha = 5 \times 10^{-3}$, the results are shown in Fig. 2, for grains subject to growth and erosion only. In the left panel, the grains have an initial size of $0.2 \mu\text{m}$ and grow until they begin to drift towards the star as their Stokes number approaches 0.1. The grains continue to grow while drifting until erosion occurs at a distance of 0.19 au. Erosion is extremely effective for ejected grains, with $s_{\text{ej}} = 1 \text{ mm}$ (R20). The aggregates, with a maximum size of 4–6 metres, are rapidly eroded to sizes of a few centimetres. Then, the grains reach an equilibrium between growth and erosion, and drift slowly from 0.19 au inwards. For comparison, the green, orange and red lines represent the evolution of a grain considering growth and fragmentation, but no erosion. The fragmentation threshold is set to 20, 40 and 80 m s^{-1} respectively. Even a high fragmentation threshold of 80 m s^{-1} (a value completely unrealistic for most of the disc, resembling pure growth), the fragmentation threshold is reached before the erosion threshold. Therefore, fragmentation is always more effective in destroying dust grains when a realistic value is used.

We can also consider what would happen if the dust is trapped and can no longer drift to be accreted onto the star. The answer is shown in the right panel of Fig. 2. Fragmentation is still effective in limiting the grain size. In the case without fragmentation, erosion is unable to balance out growth. There is a small difference around $s = 0.1 \text{ m}$ due to erosion, which reduces the growth rate without completely countering it, affecting the final grain size somewhat. However, in this case, the final size is of little importance since the grains are trapped, making it possible for them to form larger objects of more than one kilometre at later stages.

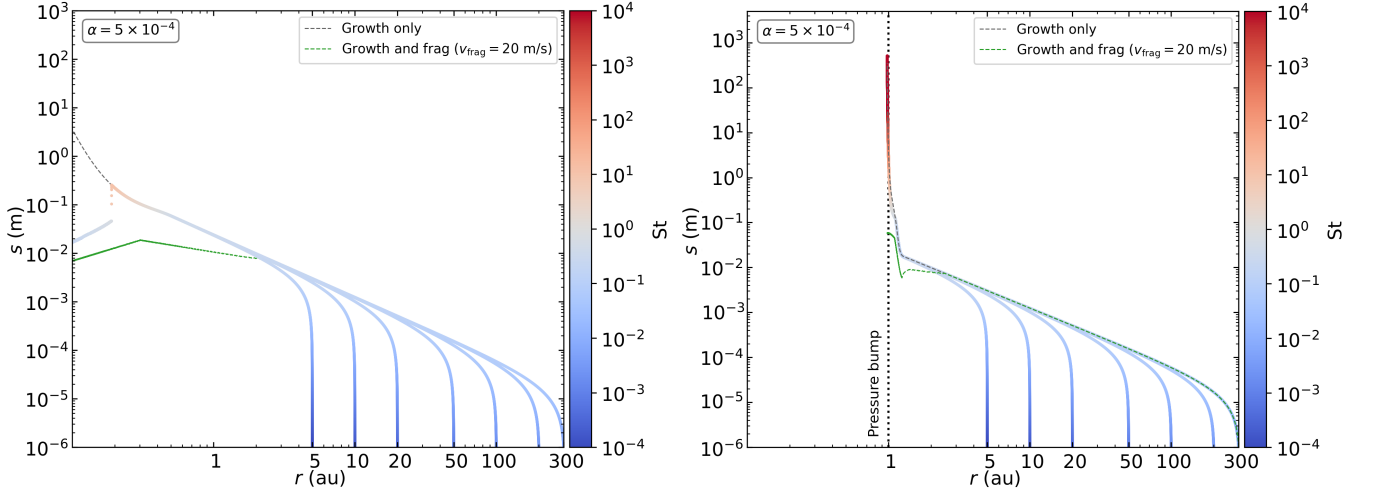


Fig. 3. Left: Same as Fig. 2, but with $\alpha = 5 \times 10^{-4}$ and only one fragmentation threshold.

The reason why erosion is almost absent within a dust trap is simple. Erosion depends on Δv , and in a dust trap, the dust-to-gas ratio ($\varepsilon = 1$ in our case) is greater than the typical value of 1%. Taking into account back-reaction, dust tends to make the gas orbit faster and vice versa, reducing Δv . Additionally, as the dust density $\rho_d = \varepsilon \rho_g$ increases, the growth rate is multiplied by 100 (Eq. (1)). These two factors work against erosion and prevent it from occurring or at least having a significant impact.

We then perform the same simulations, but with $\alpha = 5 \times 10^{-4}$ shown in Fig. 3. The results are qualitatively the same. In the left panel, the grains have the same initial size and grow until they begin to drift towards the star. The grains are eroded at the same distance of 0.19 au. Erosion is also effective, but with $\alpha = 5 \times 10^{-4}$, grain growth is less efficient because of lower relative velocities when the viscosity is lower. The aggregates, with a maximum size of 50 centimetres, are eroded to sizes of a few centimetres, reach the equilibrium and drift inwards. The green line represents the evolution when fragmentation is taken into account, with a threshold set to 20 m s^{-1} . Fragmentation is still more effective in destroying dust grains when such a realistic value is used. Higher thresholds with this α lead to an evolution resembling the pure growth case. Nevertheless, erosion reduces the size of the grains by one order of magnitude, compared to roughly 3 when $\alpha = 5 \times 10^{-3}$.

Within the dust trap, shown on the right panel, erosion is almost absent. The case with erosion does not differ from the case with pure growth, and only two scenarios are identified. If the threshold is low enough, grains are destroyed by fragmentation. Otherwise, dust grains can grow freely.

We also performed tests considering porosity (see Michoulier & Gonzalez 2022, for its implementation), and we observed no significant change in the appearance of erosion (not shown). We ran a simulation with $\alpha = 5 \times 10^{-5}$, but grain growth is so slow that dust barely reaches sizes of a few centimetres. Erosion still appears, but the dust size is only divided by a factor of two to three. In this case, the limiting factor to the grain size is the very low growth rate.

4.3. 3D study

We want to check now if we obtain the same behaviour with 3D simulations. We choose a high velocity threshold of $v_{\text{frag}} = 80 \text{ m s}^{-1}$, for which fragmentation is hardly restrictive and our

1D simulations showed that it still dominates over erosion. Figure 4 shows the radial grain size distribution coloured with the dust-to-gas ratio ε , for four simulations at time $t = 100 \text{ yr}$. The top left panel corresponds to growth only, top right to growth and fragmentation, bottom left to growth and erosion, and bottom right to growth, fragmentation and erosion. We see that the simulation with growth is able to form large grains up to the decimetre between 0.5 and 2 au. Simulations with fragmentation are identical when erosion is turned on or off (right panels). This means fragmentation is the dominant mechanism to destroy grains. When comparing the simulation with growth only and the one with erosion, the impact of erosion appears only when sizes are larger than 3 cm, interior to 1 au. This is qualitatively similar to our 1D simulations, however here grains start to be eroded at larger distances ($\sim 0.9 \text{ au}$). This is due to larger volume densities ρ_g in the midplane of the 3D disc compared to the 1D case. Moreover, fragmentation destroys grains at roughly the same size and at the same distance both in 1D and 3D. Aggregates of decimetre size are still present, as in the growth-only simulation. For the simulations with fragmentation, the peak in the size profile corresponds to the distance where $v_{\text{rel}} = v_{\text{frag}}$, and the plateau inwards shows an equilibrium between growth and fragmentation (Vericel et al. 2021).

The simulation with growth only is the one where the inner region is the less dust-enriched, with $\varepsilon < 10^{-1}$. One should note that dust has been lost to the star due to radial drift in the very inner region. On the contrary, the ones with fragmentation have $\varepsilon \sim 2 \times 10^{-1}$ at 0.6 au. Fragmentation helps grains to stay in the disc because their sizes become smaller the closer they are to the star, which means they will be more coupled to the gas and less prone to drift. With erosion only, the region between 0.6 and 1 au has $\varepsilon \sim 10^{-1}$. Erosion can thus help the inner region to increase the local dust-to-gas ratio, but it is not as efficient as fragmentation. Outside 2 au, the size profiles of all simulations are very similar, as neither fragmentation nor erosion affect dust growth.

These simulations support the results from our 1D simulations. Moreover, they show that when accounting for fragmentation, erosion is not present even with $v_{\text{frag}} = 80 \text{ m s}^{-1}$, which means it can be ignored during dust evolution and growth of aggregates.

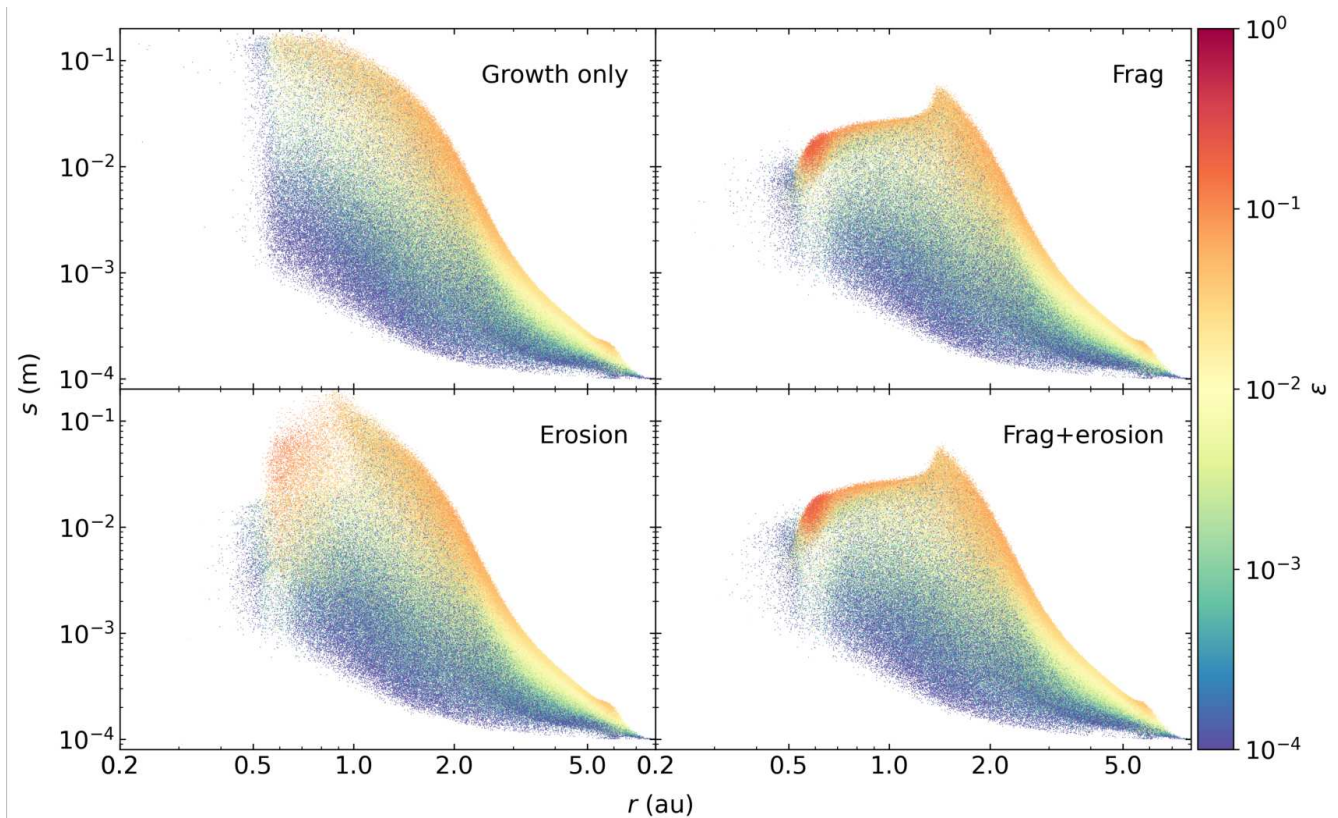


Fig. 4. Comparison between simulations in the (r, s) plane at $t = 100$ yr with growth only top left, growth and fragmentation top right with $v_{\text{frag}, \text{Si}} = 80 \text{ m s}^{-1}$, growth and erosion bottom left and growth, fragmentation and erosion bottom right. The colour gives the dust-to-gas ratio.

5. Discussion

5.1. Caveats

The main limitations arise from our model of dust growth, as we use a 3D code that eliminates most of the approximations done with the 1D Code PAMDEAS. However, since we use the mono-disperse approximation for dust growth, we do not track all the smaller grains ejected from larger bodies due to erosion. This is not very important as we want to track the evolution of the largest grains, since fragmentation always appears before erosion. In addition, the mono-disperse approximation only considers collisions of equal-size grains. Unequal-size grains have relative settling and drifting velocities, acting as additional sources of collisions. The SPH formalism naturally produces a spread in Δv , resulting in a spread in v_{rel} as well, similar to the velocity distributions in Windmark et al. (2012b); Garaud et al. (2013). Nevertheless, our approximation can not account for high-mass-ratio collisions, which have been found to result in net growth even at v_{rel} as high as 70 or 80 m s^{-1} (Teiser & Wurm 2009; Kothe et al. 2010; Windmark et al. 2012a; Wada et al. 2013; Meisner et al. 2013).

Aeolian erosion is a continuous process and one may wonder whether the discrete nature of particle collision would hinder the comparison between both processes. This is not a problem in numerical simulations, where time is incremented by a finite quantity, the timestep. Even when the time between collisions is long, it is still much shorter than a single timestep (e.g. Garcia & Gonzalez 2020). Both processes are thus taken into account simultaneously in our simulations.

Another issue is the fact that we do not take into account porosity in the model. This could play a role, as porous grains

tend to form larger aggregates while being less sensitive to fragmentation. A model of erosion taking into account porosity would be more precise in capturing dust evolution. But we do not think this will change the results significantly because fragmentation will remain the limiting factor.

Lastly, in the erosion model, β_{eros} is still not very well constrained for different kinds of material and more experimental measurements would be needed, although progress has been made in recent work (Demirci et al. 2020; Schönau et al. 2023). The model also assumes that all ejected grains have the same size, while in reality, all sizes should be considered.

5.2. Importance of erosion

We see in this paper that fragmentation is always the first process to destroy grains before erosion for $v_{\text{frag}} = 20 \text{ m s}^{-1}$. Smaller fragmentation thresholds like 10 or 15 m s^{-1} only strengthen fragmentation, thus decreasing the effect of erosion, while larger fragmentation threshold can be considered less realistic, both with $\alpha = 5 \times 10^{-3}$ and $\alpha = 5 \times 10^{-4}$. Moreover, we use the size $s_{\text{ej}} = 1 \text{ mm}$ adopted by R20 and G20, which makes erosion more effective. Therefore, we can safely say that erosion can be completely neglected in dust models when $\alpha = 5 \times 10^{-3}$. For $\alpha = 5 \times 10^{-4}$, the only fragmentation considered is $v_{\text{frag}} = 20 \text{ m s}^{-1}$, because higher v_{frag} are extremely similar to pure growth. The difference of sizes just before and after erosion in this case is also smaller, by an order of magnitude, reducing the impact of erosion on dust evolution. Finally, adding a pressure bump at 1 au did not help erosion to appear, despite the fact that grains grow up to one kilometre. Erosion can therefore be neglected in all cases when fragmentation is considered. For a very low-

viscosity disc, erosion could still be ignored, as grains growth would be very slow and large sizes wouldn't be reached. However, it is worth mentioning that if larger boulders or planetesimals are formed or captured, erosion would still be important in grinding them down in the inner disc region, as discussed by Grishin et al. (2019); Rozner et al. (2020).

6. Summary and conclusion

In this paper, we discuss the importance of erosion in the evolution of dust in protoplanetary disc. We first present the way we modelled radial drift in a 1D code to capture accurately the effect even if the disc is stationary and the gas is not evolving. We then present how erosion has been treated based on R20 and G20, giving the two important equation to implement in the codes. We also present the model to take into account both growth and fragmentation from Stepinski & Valageas (1997), Laibe et al. (2008), Garcia (2018), Vericel et al. (2021), Michoulier & Gonzalez (2022). We perform some tests to be sure PAMDEAS reproduces some of the key results presented in R20 and G20. We then perform simulations with the same model implemented in both the PAMDEAS and PHANTOM codes. We show that erosion is negligible when fragmentation is taken into account with realistic fragmentation thresholds. Both codes give the same results. When considering a pressure bump, erosion is still not efficient at destroying grains. We then discuss the main caveats of this study and a discussion of the insignificance of erosion. To conclude, erosion can be neglected in models of dust evolution accounting for fragmentation, bouncing, or any other mechanism that limits the dust sizes to a couple of centimetres in the very inner region of a protoplanetary disc. Usually, such short distances of a fraction of au are not considered when doing simulations and erosion can be safely neglected from a dust evolution perspective.

Acknowledgements. We thank Daniel J. Price for useful discussion and advice and the anonymous referee for their suggestions. The authors acknowledge funding from ANR (Agence Nationale de la Recherche) of France under contract number ANR-16-CE31-0013 (Planet-Forming-Disks) and thank the LABEX Lyon Institute of Origins (ANR-10-LABX-0066) for its financial support within the Plan France 2030 of the French government operated by the ANR. This research was partially supported by the Programme National de Physique Stellaire and the Programme National de Planétologie of CNRS (Centre National de la Recherche Scientifique)/INSU (Institut National des Sciences de l'Univers), France. We gratefully acknowledge support from the PSMN (Pôle Scientifique de Modélisation Numérique) of the ENS de Lyon for the computing resources. This project has received funding from the European Union's Horizon 2020 research and innovation programme under the Marie Skłodowska-Curie grant agreements No 210021 and No 823823 (DUSTBUSTERS). Figures were made with the Python library `matplotlib` (Hunter 2007).

References

- Auffinger, J. & Laibe, G. 2018, MNRAS, 473, 796, aDS Bibcode: 2018MNRAS.473..796A
- Barge, P. & Sommeria, J. 1995, A&A, 295, L1
- Blum, J. & Wurm, G. 2000, Icarus, 143, 138
- Blum, J. & Wurm, G. 2008, ARA&A, 46, 21
- Brauer, F., Henning, T., & Dullemond, C. P. 2008, A&A, 487, L1
- Demirci, T., Schneider, N., Steinpilz, T., et al. 2020, MNRAS, 493, 5456
- Dominik, C. & Tielens, A. G. G. M. 1997, ApJ, 480, 647, aDS Bibcode: 1997ApJ...480..647D
- Drażkowska, J., Windmark, F., & Dullemond, C. P. 2014, A&A, 567, A38
- Garaud, P., Meru, F., Galvagni, M., & Olczak, C. 2013, ApJ, 764, 146
- Garcia, A. 2018, Phd thesis, Université de Lyon, available at <https://theses.hal.science/tel-01977317/document>, in French
- Garcia, A. J. L. & Gonzalez, J.-F. 2020, MNRAS, 493, 1788
- Gonzalez, J.-F., Laibe, G., & Maddison, S. T. 2017, MNRAS, 467, 1984
- Gonzalez, J.-F., Laibe, G., Maddison, S. T., Pinte, C., & Ménard, F. 2015, Planet. Space Sci., 116, 48
- Grishin, E. & Perets, H. B. 2015, ApJ, 811, 54
- Grishin, E., Perets, H. B., & Avni, Y. 2019, MNRAS, 487, 3324
- Grishin, E., Rozner, M., & Perets, H. B. 2020, ApJ, 898, L13
- Gunkelmann, N., Ringl, C., & Urbassek, H. M. 2016, A&A, 589, A30
- Heim, L.-O., Blum, J., Preuss, M., & Butt, H.-J. 1999, Phys. Rev. Lett., 83, 3328
- Hunter, J. D. 2007, Computing in Science & Engineering, 9, 90
- Kataoka, A., Tanaka, H., Okuzumi, S., & Wada, K. 2013, A&A, 557, L4
- Kobayashi, H. & Tanaka, H. 2010, Icarus, 206, 735
- Kothe, S., Güttler, C., & Blum, J. 2010, ApJ, 725, 1242
- Kretke, K. A. & Lin, D. N. C. 2007, The Astrophysical Journal, 664, L55
- Laibe, G., Gonzalez, J. F., Fouchet, L., & Maddison, S. T. 2008, A&A, 487, 265
- Li, R., Youdin, A. N., & Simon, J. B. 2019, ApJ, 885, 69, aDS Bibcode: 2019ApJ...885...69L
- Loren-Aguilar, P. & Bate, M. R. 2015, MNRAS, 453, L78, arXiv: 1507.05499
- Meheut, H., Keppens, R., Casse, F., & Benz, W. 2012, A&A, 542, A9
- Meisner, T., Wurm, G., Teiser, J., & Schywek, M. 2013, A&A, 559, A123
- Michoulier, S. & Gonzalez, J.-F. 2022, MNRAS, 517, 3064
- Okuzumi, S., Tanaka, H., Kobayashi, H., & Wada, K. 2012, ApJ, 752, 106
- Okuzumi, S., Tanaka, H., & Sakagami, M.-a. 2009, ApJ, 707, 1247
- Ormel, C. W., Spaans, M., & Tielens, A. G. G. M. 2007, A&A, 461, 215
- Paraskov, G. B., Wurm, G., & Krauss, O. 2006, ApJ, 648, 1219
- Perets, H. B. & Murray-Clay, R. A. 2011, ApJ, 733, 56
- Pfalzner, S. & Bannister, M. T. 2019, ApJ, 874, L34
- Pfalzner, S., Paterson, D., Bannister, M. T., & Portegies Zwart, S. 2021, ApJ, 921, 168
- Price, D. J., Wurster, J., Tricco, T. S., et al. 2018, Publications of the Astronomical Society of Australia, 35, e031
- Ringl, C., Bringa, E. M., Bertoldi, D. S., & Urbassek, H. M. 2012, ApJ, 752, 151
- Rozner, M., Grishin, E., & Perets, H. B. 2020, MNRAS, 496, 4827
- Schäfer, U., Yang, C.-C., & Johansen, A. 2017, A&A, 597, A69
- Schönaul, L., Teiser, J., Demirci, T., et al. 2023, A&A, 672, A169
- Shakura, N. I. & Sunyaev, R. A. 1973, A&A, 24, 337
- Shao, Y. & Lu, H. 2000, Journal of Geophysical Research, 105, 22437
- Stepinski, T. F. & Valageas, P. 1997, A&A, 319, 1007
- Suyama, T., Wada, K., & Tanaka, H. 2008, ApJ, 684, 1310
- Tanaka, H., Inaba, S., & Nakazawa, K. 1996, Icarus, 123, 450
- Tatsumi, M. & Kataoka, A. 2021, ApJ, 913, 132
- Teiser, J. & Wurm, G. 2009, MNRAS, 393, 1584
- Vericel, A. & Gonzalez, J.-F. 2020, MNRAS, 492, 210
- Vericel, A., Gonzalez, J.-F., Price, D. J., Laibe, G., & Pinte, C. 2021, MNRAS, 507, 2318, aDS Bibcode: 2021MNRAS.507.2318V

- Wada, K., Tanaka, H., Okuzumi, S., et al. 2013, A&A, 559, A62
- Weidenschilling, S. J. 1977, MNRAS, 180, 57, aDS Bibcode: 1977MNRAS.180...57W
- Weidenschilling, S. J. & Cuzzi, J. N. 1993, in Protostars and Planets III, ed. E. H. Levy & J. I. Lunine, 1031
- Whipple, F. L. 1972, in From Plasma to Planet, ed. A. Elvius, 211
- Williams, J. P. & Best, W. M. J. 2014, ApJ, 788, 59, aDS Bibcode: 2014ApJ...788...59W
- Windmark, F., Birnstiel, T., Güttler, C., et al. 2012a, A&A, 540, A73
- Windmark, F., Birnstiel, T., Ormel, C. W., & Dullemond, C. P. 2012b, A&A, 544, L16
- Wurm, G., Blum, J., & Colwell, J. E. 2001, Phys. Rev. E, 64, 046301
- Yang, C.-C., Johansen, A., & Carrera, D. 2017, A&A, 606, A80
- Youdin, A. & Johansen, A. 2007, ApJ, 662, 613
- Youdin, A. N. & Goodman, J. 2005, ApJ, 620, 459, aDS Bibcode: 2005ApJ...620..459Y